Available online at www.sciencedirect.com

ScienceDirect

Energy Procedia 94 (2016) 329 – 338

Energy Procedia

[S1]13th Deep Sea Offshore Wind R&D Conference, EERA DeepWind'2016, 20-22 January 2016, Trondheim, Norway

Maximum loads on a one degree of freedom model-scale offshore wind turbine

Loup Suja-Thauvin*[ab], Jørgen Ranum Krokstad[ab], Joakim Fürst Frimann-Dahl[b]

[a]*Statkraft AS, Offshore Wind Department,Sluppenveien 17B, Trondheim 7005, Norway*
[b]*NTNU, Department of Marine Technology, Trondheim 7491, Norway*

Abstract

This paper presents the results of an experiment carried out in a wave flume aiming at reproducing a 50-year wave condition on an extra-large bottom-fixed offshore wind turbine mounted on a monopile. The model is a stiff cylinder mounted on a spring allowing rotation of the system around its base only in the wave propagation direction. Under these conditions, the turbine is assumed to be idling, and the damping ratio of the system is 2.4%. The overturning moment at the base of the cylinder is measured, and it is found that the maximum responses are recorded when long steep breaking or near-breaking waves hit the cylinder and excite the first eigenperiod of the structure. For a selected event involving a breaking wave, the response of the system is compared to numerical simulations using the FNV method. The higher order excitation loads from the FNV are approximated as sinusoid pulse loads, and it is shown that since the duration of these pulses lies close to the eigenperiod of the structure, they suffice to trigger the first mode motion, without the need for a slamming model. A consequence of the low damping is that if the structure has been previously excited at its 1st mode (linearly or by higher order phenomena such as springing), the structure can already have a motion that adds up to the transient response to the pulse loads. The findings of this study also challenge some of the load models currently used by the industry to estimate the response of offshore wind turbines during extreme events.

Peer-review under responsibility of SINTEF Energi AS

Keywords: extra-large monopile, 50-year storm, low damping

1. Introduction

Offshore wind turbines in extreme weather often encounter steep or breaking waves that produce high response loads threatening the structural integrity of the foundation. Under these conditions the blades are typically pitched so that the turbine is idling, decreasing the total damping on the first mode for the whole structure.

Peer-review under responsibility of SINTEF Energi AS

doi:10.1016/j.egypro.2016.09.191

During model tests performed in a wave flume at the Norwegian University of Science and Technology (NTNU) in Trondheim in April-May 2015, a one degree of freedom model composed of a stiff cylinder mounted on a rotational spring was exposed to 50-years wave conditions. Due to low damping, a lot of first mode oscillation could be observed through the experiment, and it was not clear whether these oscillations were due to linear excitation, non-linear excitation or slamming events. The structure was hit by a number of steep and breaking waves that produced oscillations of the whole structure and induced the maximum recorded loads.

This paper challenges the physics behind the maximum events and how the low damping has a primary effect on them. It is organized as follow: Section 2 is a short presentation of the experiment and section 3 is a presentation of the numerical model used to represent the system and the hydrodynamic loads. In section 4 we try to match the experimental results with a simple model that can explain the behavior of the turbine and how the maximum loads are reached, and section 5 concludes on the findings of this paper.

2. Presentation of the experiments

This model test was carried out in the small wave flume at NTNU in April and May 2015. This flume is 28m long and 2.5m wide with a constant water depth. One end of the flume is fitted with a perforated parabolic absorbing beach and the other end is equipped with a piston-type wave maker, consisting on a flat plate forced into translational motion by an electric actuator. At about 15m from the wave maker, a pit has been constructed where the model is fixed.

The model is a representation of a bottom-fixed extra-large offshore wind turbine mounted on a monopile with a scale of 1:48. It is a stiff cylinder 1.54m long with a 0.144m diameter and 6mm thick, attached to a force and moment transducer via an intermediate piece that behaves as a spring. These parts are dimensioned so that the bottom of the cylinder is exactly at the mudline. The transducer is then mounted on a stiff truss structure which is solidly anchored to the ground. The spring has been designed to model the stiffness of the soil, and enables the cylinder to rotate around its base in the wave direction but not in the transverse direction. The stiffness of the spring is 3300 Nm/rd. A mass of 5.04kg was added to the top of the model in order to model the mass of the rotor-nacelle assembly and get the correct eigenperiod for the system. The values given in this paragraph are model scale values; their full-scale equivalent is given in table 1.

Decay test were performed on the structure, and it was found that the whole system (with the correct water depth) had a damping ratio of 2.4%. [1] and [2] estimated the total damping of offshore wind turbines based on rotor-stop sequences for five wind parks and found mean damping ratios varying between 2.3 and 2.5%. The water depths of the considered wind parks were between 6 and 27m, which shows that these damping ratios are realistic for a wide range of water depths. On a different wind farm, [3] found that for low wind speeds and with the tuned mass damper blocked, the damping ratio was 1.1%. For the same turbine, [4] found that fore-aft damping ratios could vary from 1.7 to 2.8% depending on the wind speed, with the highest values corresponding to the highest wind speeds and with the tuned mass damper on. The values used in the presented experiments lie within the range of full-scale wind turbine in idling conditions.

Two different water depths with 8 sea states and 20 seeds per sea state were run. Only one run is studied in details in this paper, and was aimed at modelling 50-year storm at the Dogger Bank Creyke Beck B site [5]. The waves were randomly generated following a JONSWAP spectrum with a significant wave height $H_S = 0.171$m and a spectral peak period $T_P = 1.62$s at a water depth of 0.625m (corresponding to full scale values of $H_S = 8.22$m, $T_P = 11.25$s and $h = 30$m). Under these conditions, the turbine will be idling, so no aerodynamic modelling is implemented.

The tank flume was equipped with pairs of capacitance wave gauges at different positions along its length, which were used to measure the wave elevation input into the numerical model (see section 3.2.1). Two accelerometers were placed at the top of the cylinder and confirmed that the model experienced motion only in the wave direction. The force and moment transducer aforementioned was used to calculate the response of the structure to the incoming waves. Two cameras recorded the whole duration of the test enabling a visual check of the wave. Focus was on whether the wave had broken when exciting the cylinder.

Table 1. characteristics of the model test

	Diameter	Water depth	Rotational stiffness	Damping ratio	Eigenperiod
Full scale	6.9m	30m	1.75e7 kNm/rad	2.4%	3.89s
Model scale	144mm	625mm	3300 Nm/rad	2.4%	0.562s

Table 1 shows the characteristics of the model and their equivalent in full scale. A more exhaustive description of the model test can be found in [6].

3. Description of the numerical model

3.1. Model of the structure

The structure is represented by the classical single degree of freedom equation:

$$M_{hydro} = (I_P + I_A)\ddot{\theta} + C\dot{\theta} + K\theta \quad (1)$$

with M_{hydro} excitation moment due to the waves
I_P moment of inertia of the pile
I_A moment of inertia due to the added mass
C damping coefficient
K rotational stiffness of the spring
θ angular displacement of the structure

The dot over a variable means differentiation. The moment of inertia was calculated using an added mass coefficient of 1. Wavelet analysis showed small or close to negligible changes in the first mode frequency throughout all the recorded tests. The rotational stiffness was calculated based on the material and geometrical properties of the spring and tuned to fit the eigenperiod of the structure. The damping coefficient was estimated from the logarithmic decrement of the decay tests. Figure 1 shows the overturning moment measured at the base of the cylinder during the decay test and the simulation with the fitted parameters.

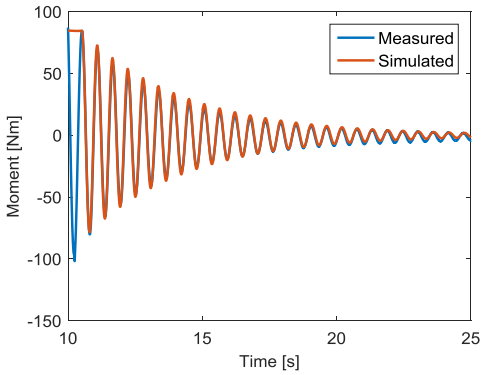

Fig 1. Decay test, experimental and numerical

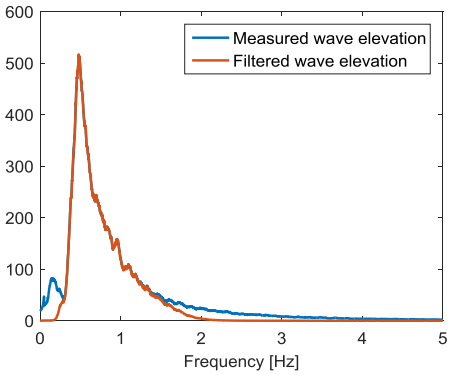

Fig 2. Spectra of the filtered and unfiltered measured wave elevation

3.2. Hydrodynamic load model

The input to equation (1) is the hydrodynamic excitation loads, which were calculated from the wave elevation measured during the model tests. The first part of this section will present the simple method used to obtain a linear

wave time series from the measured wave elevation (the concept of a linear wave time series and the reason for this being required are explained in the next section). The linear wave time series is then used as an input to the load model, which is developed in the second part of this section.

3.2.1. Linear input wave

The model used in this analysis is the FNV model, a weakly nonlinear model which will be presented in the next section. This model calculates 2nd and 3rd order hydrodynamic loads (in terms of wave steepness) from linear wave kinematics. If the wave kinematics used as input contain higher order terms, for instance 2nd order wave kinematics, 2nd order hydrodynamic loads would be calculated from two contributions: (i) from the linear term of the FNV (see first line of equation (3)) applied to 2nd order wave kinematics, and (ii) from the 2nd order term of the FNV (see second line of equation (3)) applied to linear wave kinematics. This would be inconsistent and produce conservative hydrodynamic excitation loads.

As a wave travels from the wave-maker to the model, non-linearities start to develop, and even more so due to the shallow waters considered. These are therefore found in the measured wave and should be removed before inputting the wave elevation into the FNV model. For the present paper, an attempt to linearize the measured wave elevation was made by filtering out the difference- and the sum-frequencies present in the wave spectrum.

The waves due to difference-frequencies do not present a major difficulty, as they lie distinctively from the linear wave in the spectrum. It can be seen in figure 2 how applying a high-pass filter to the measured wave elevation suffices to eliminate the difference-frequencies.

The waves due to second-order sum-frequencies require a much more elaborated method. Most of the energy from sum-frequency waves lies at about twice the spectral peak period which in a JONSWAP spectrum also contains energy from linear waves. Completely filtering out the energy at those frequencies would therefore result in a loss of information coming from the linear waves. For the present analysis, a simple method consisting in applying a Butterworth low-pass filter was used. The cut-off frequency, as suggested in [7] is defined by

$$\omega_{cut-off} = \sqrt{2g/H_S} \tag{2}$$

where g is the gravitational acceleration. Figure 2 shows the spectrum of the measured wave elevation in blue, and the same spectrum once the filtering has been applied. As can be seen from the figure, there is a significant difference between the filtered and unfiltered spectra at high frequencies (so-called tail of the spectra). According to [8], weakly nonlinear models are strongly dependent on the cutoff frequency, which means that the results from the present analysis must be used carefully. However, the results presented here are qualitative, and attention is given to the phasing of nonlinear terms rather than their amplitude. More accurate ways of obtaining the linear wave elevation from a measured time series can be found in [9] or [10].

3.2.2. Excitation loads: FNV model

The model used to calculate the excitation loads is the Faltinsen-Newman-Vinje model (hereafter referred as FNV, see [11]), which accounts for loads up to 3rd order in terms of wave steepness (referred as ϵ hereafter). The FNV was developed in the 90s when ringing was first observed in basin experiments (see [12]) first for regular waves and further developed for irregular waves by [13]. The hydrodynamic excitation force calculated by the FNV method as found in [13] is given by the following equation:

$$\begin{aligned} F_{FNV} = \; & 2\pi\rho R^2 \textstyle\int_{-h}^{0} u_t(z)dz && O(\epsilon) \\ & + 2\pi\rho R^2 u_t|_{z=0}\zeta^{(1)} + \pi\rho R^2 \int_{-h}^{0} [2w(z)w_x(z) + u(z)u_x(z)]dz && O(\epsilon^2) \\ & + \pi\rho R^2 \left[\zeta^{(1)}\left(u_{tz}\zeta^{(1)} + 2ww_x + uu_x - \frac{2}{g}u_t w_t\right) - \left(\frac{u_t}{g}\right)(u^2+v^2)\Big|_{z=0}\right] && O(\epsilon^3) \\ & + \pi\rho\frac{R^2}{g}u^2 u_t|_{z=0}\beta\left(h/R\right) && O(\epsilon^3) \end{aligned} \tag{3}$$

Where ρ is the water density, u and w are the horizontal and vertical first order velocity components, $\zeta^{(1)}$ is the first order wave elevation, h is the mean water depth, R is the cylinder radius, and subscripts indicate differentiation. β is given by

$$\beta\left(h/R\right) = \int_0^{h/R} \left(3\Psi_1(Z) + 4\Psi_2(Z)\right) dZ \tag{4}$$

with Ψ_1 and Ψ_2 defined in [13]. These functions represent the steady state and near field non-linear interaction with the cylinder for a deeply penetrating and constant diameter cylinder. The slenderness parameter, δ, has been omitted for simplicity. It is shown in [14] that all terms of equation (3) are of the order of δ^2. The FNV formulation assumes that $\epsilon \sim \delta$, which is equivalent to saying that the wave amplitude is close to the cylinder diameter. In the implementation of the model, the deep water assumption was used for β as indicated in [13], giving $\beta = 4$.

The FNV equations do not model any breaking wave loading effect, i.e. they do not model load events related to rapid change of added mass impacting the cylinder. The reason for using this model, as will be discussed in detail later, is to show that the higher order excitation loads (proportional to ϵ^2 and ϵ^3) can predict the response measured during the experiments.

The original formulation for the FNV, as shown in equation (3), gives a lumped force whose application point is at the mean free surface. The overturning moment at the mudline is then simply obtained by multiplying this force by the arm. In the present model, the two terms of equation (3) that require integration from the mudline to the mean water level, have been calculated as a distributed force. Each contribution has been multiplied by the corresponding arm to obtain the distributed moment. The first term for the overturning moment, which is equivalent to the inertia term of the classical Morison load, is then

$$Mf1 = 2\pi\rho R^2 \int_{-h}^{0} \left(z u_t(z)\right) dz \tag{5}$$

And the second term is

$$Mf21 = \pi\rho R^2 \int_{-h}^{0} z\left[2w(z)w_x(z) + u(z)u_x(z)\right] dz \tag{6}$$

The first term of second order of equation (3) corresponds to the contribution of the linear potential integrated from the mean water depth to the first order wave elevation. In the present model, this force will be applied at the mean water level and the moment from this force will be

$$Mf2Free = 2\pi\rho R^2 u_t\big|_{z=0} \zeta^{(1)} \cdot h \tag{7}$$

The terms in the third and fourth line of equation (3) are third order term and will be multiplied by the mean water depth to obtain moments respectively named $Mf31$ and $Mf3Xsi$.

The FNV model was initially developed for infinite water depth. Under the current setting, with a water depth of 30m and a spectral peak period of 11.25s, the ratio between water depth and wavelength is about 0.18, which according to [15] is in the intermediate water depth range. An attempt to account for some finite water depth effects was made by using a finite water potential when calculating the wave kinematics, integrating $Mf1$ and $Mf21$ over a finite depth and using the finite water depth dispersion relationship (found for instance in [16]).

The FNV is known to overestimate the loads, and it is inconsistent to use finite water depth kinematics since the formulas were developped assuming a deep water potential. However, as mentioned in section 3.2.1, this analysis aims at giving a qualitative explanation of the loading process with special focus on the phasing of different excitation loads and the response. The results, as will be seen in figure 3, fit the experiment sufficiently well to be considered valid as a parametric and efficient non-linear model.

4. Numerical results

The FNV model was run with all the modelled sea states. It is known to be too conservative in general, but in the present analysis there were some events that were accurately depicted by the FNV. The maximum moment recorded for the sea state H_S = 0.171m, T_P = 1.62s and h = 0.625m occurred at about t = 994s and is shown in figure 3. During this event, it was visible from the video recording that a breaking wave impacted the turbine, and that the turbine started oscillating at its eigenperiod. In [17], slamming tests were carried out in a wave flume, and it was shown that the time duration of the impact is very small compared to the first eigenperiod of the structure. According to classical structure theory (see for example [18] p47), this will not create significant response of the system in its first mode compared to the quasi-static response due to non-breaking waves. In the following we try to show that non-impact higher order loads alone can explain the observed first mode motion.

It appears from this figure 3 that the FNV gives a good approximation of the maximum moment whereas the Morison model (applied here with the same linear wave kinematics as the FNV model and with Wheeler stretching) underpredicts it. This is described in [16]. As the structure continues oscillating at its eigenfrequency, the FNV model starts to clearly overpredict the results while a closer fit is obtained with the Morison equation. As this paper analyses the maximum load and the mechanism that triggers the first mode motion of the structure, we focus on the first seconds of the event described here, which are correctly depicted by the FNV.

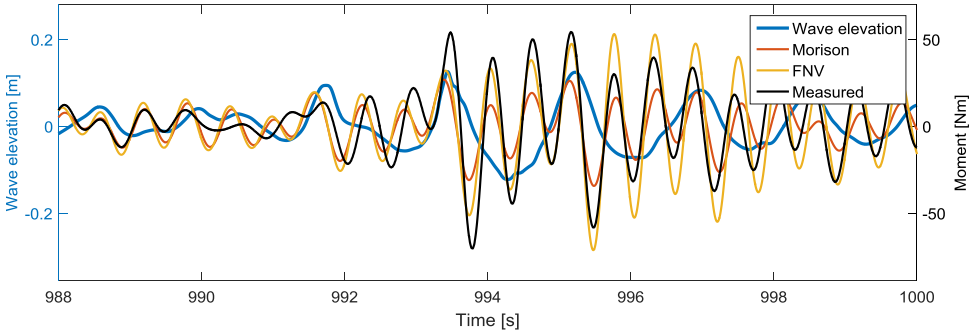

Fig 3. Maximum recorded event from measurements and simulated, for H_S = 0.171m, T_P = 1.62s and h = 0.625m

Figure 4 shows the different terms of the FNV for the maximum event ($Mf1$ is not shown as it is already clear from figure 3 that the Morison equation alone is not able to fully capture the first mode motion). From this figure one can see that $Mf2Free$, $Mf31$ and $Mf3Xsi$ experience a dramatic increase around 993s. These moments are referred to later in this paper as higher order moments. As a first approximation, these three excitation loads are represented by a pulse load with a sinusoidal shape and variying periods (by pulse load we refer to a load that has zero amplitude except for a duration of the order of magnitude of a characteristic period of the system or smaller, like the load showed in figures 5 and 6). The aim of this approximation is to assess whether these loads are able to trigger the 1st mode motion.

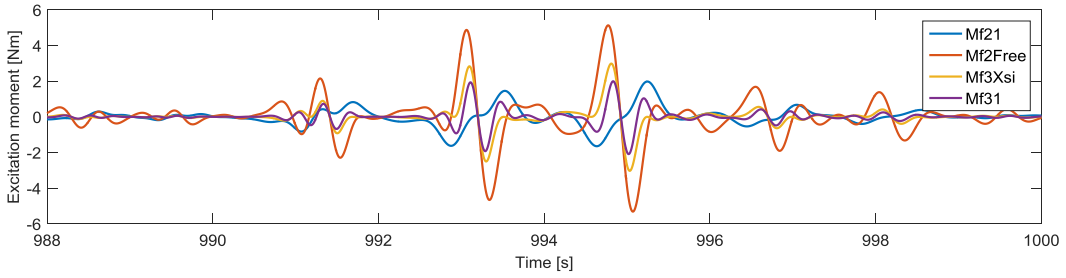

Fig 4. Excitation moments derived from the FNV

A pulse load of sinusoidal shape and arbitrary amplitude M_i is input to the numerical model. This simulation is ran many times with the pulse load duration t_d as a parameter. The maximum measured response is then divided by the static response (response to a constant load of same amplitude), giving the maximum dynamic load factor DLF_{max} (see [18]). Figure 5 shows the maximum dynamic load factor as a function of the pulse load duration (on the x axis, the load duration has been normalized by the eigenperiod of the system). The important point of this figure is that one can compare relative values of the response of the system for different duration of the pulse. Trying to fit a sinusoidal shape on the loads of figure 4, we find that the pulse loads equivalent to $Mf2Free$, $Mf31$ and $Mf3Xsi$ have durations of 0.6s, 0.45s and 0.36s respectively. With an eigenperiod of 0.56s, that gives for $Mf2Free$, $Mf31$ and $Mf3Xsi$ an amplification of 2.8, 2.2 and 1.7 respectively. This shows that for a load duration close to the eigenperiod of the system, the response will experience a significant amplification, which can partly explain the high values of the overturning moment after a steep wave.

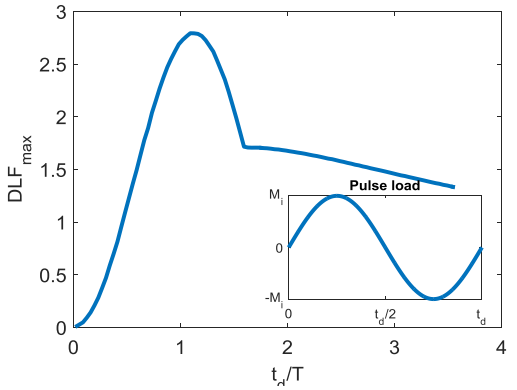

Fig 5. DLF max depending on pulse load duration

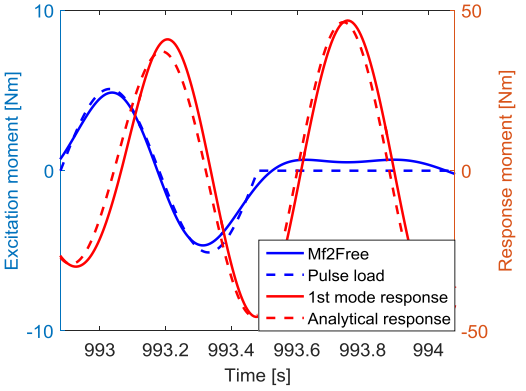

Fig 6. Comparison between the analytical response to a pulse load and the measured 1st mode response

In order to verify the assumption just formulated, an attempt to separate the 1st mode motion from the total response was made. In theory, since the model is a stiff cylinder mounted on a rotational spring, it should have only one degree of freedom and therefore only one eigenmode. However, due to the impossibility of having an infinitely stiff structure in reality, a second mode could be measured with a 2nd eigenfrequency lying around 80 Hz. It should be noted that this second mode has no full-scale meaning and is therefore not representative of the 2nd mode of a full-scale turbine. The response at the second mode was also extracted and contributed very little to the total moment, but it was seen by comparing it to the video recording that slamming events triggered second mode motion. This can also be seen in the third plot of figure 7, where the second mode response experiences a sudden increase when the breaking wave impacts the model.

In the following part, we focus on $Mf2Free$ since it is the load that will produce the highest response, but it should be noted that the other higher order loads will also produce a dynamic amplification of the first mode motion, as was shown in the previous paragraph. It is known that for short waves, diffraction effects will reduce the 2nd order force (see [14]). For the studied event, and estimated from zero-upcrossing of the local wave period, the wave number-radius product is $kR = 0.13$, which lies within the range where $Mf2Free$ is expected to give accurate results.

Figure 7 shows the mode decomposition of the response for the maximum event. The decomposition was obtained by filtering the measured moment, and was shown to be very little sensitive to the filtering methods used.

The second plot of figure 7 shows $Mf2Free$ and the 1st mode motion response. As suggested by the previous analysis, it seems like the 1st mode motion is greatly amplified by $Mf2Free$, with a delay of about 0.16 s. This delay can be explained mathematically using the classical equation for the response of an undamped linear system, that can be found in [18]:

$$M(t) = M_0 \cos(\omega t) + \frac{\dot{M}_0}{\omega} \sin(\omega t) + \omega M_a \int_0^t f(\tau) \sin[\omega(t-\tau)] d\tau \tag{8}$$

with M the response moment of the structure
M_0 response moment at the initial state
M_a load amplitude
f load shape function
ω eigenperiod of the system

We use the same assumption for the load shape than previously, that is, that the load from 0 to td is a sinusoid of period 0.6s. From figure 4 we find that the amplitude of $Mf2Free$ which we will take as the amplitude of the sinusoidal load is about $M_a = 5Nm$ (model scale). We take as the initial conditions the situation of the structure at the upscrossing time of $Mf2Free$, around 992.9s, which gives $M_0 = -27.1Nm$ and $\dot{M}_0 = -119.5Nm \cdot s^{-1}$ (model scale). The displacement from t = 0 to t = 0.6 is then

$$M(t) = M_0 \cos(\omega t) + \frac{\dot{M}_0}{\omega} \sin(\omega t) + \omega M_a \frac{\left(2\pi/t_d\right) \sin(\omega t) - \omega t \cdot \cos(\omega t)}{2\pi/t_d} \tag{9}$$

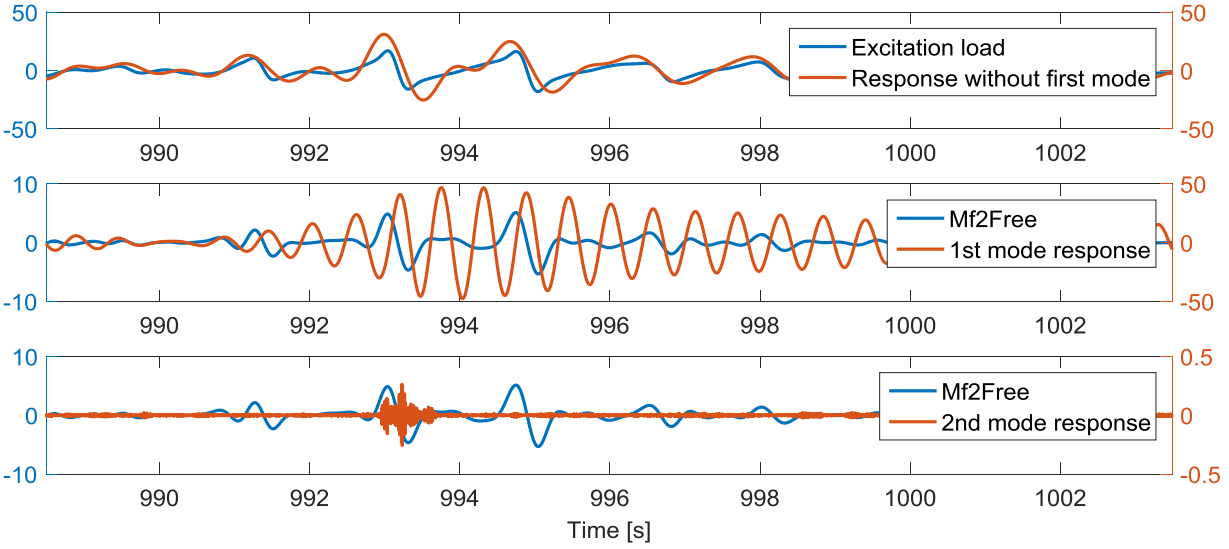

Fig 7. Response decomposition for the maximum event

Figure 6 shows the sine approximation for $Mf2Free$ and the corresponding response. The maximum for the impulsive excitation load occurs at t = 993.03s and the maximum for the analytical response occurs around t = 993.19s, which gives a time delay of 0.16s, equal to what was previously found.

After t = 0.6s, the approximated excitation load is equal to 0 and the structure starts oscillating at its eigenfrequency, without decaying since this model does not include damping. This is similar to what can be seen from figure 7, with some differences due to the fact that the shape of $Mf2Free$ is not a true sinusoid.

The value of the first maximum from figure 7 also fits well the value of figure 6. In order to have an accurate approximation of this maximum, it is critical to have the correct initial conditions. These initial conditions are determined by the history of the response, which is itself highly dependent on damping. The presented experiment

was carried with very low damping. This implies that when the first mode is excited, either by short linear waves or by a previous non-linear wave loading, it is likely that it is still oscillating when a load like the one studied in this event occurs. The response to a new sudden excitation load will then occur on top of the free decay oscillations, potentially increasing the maxima if they occur in phase.

It can be seen from figure 7 and figure 4 that a second impulsive-like 2nd order load occurs around 995s. This load has a longer duration and different initial conditions than the one studied in this analysis, both of which explain that there is not a significant increase in the 1st mode motion. This was checked with the proposed approximation and gave good quantitative results but a too high amplitude in the analytical response. This is in agreement with figure 3, where it can be seen that the FNV method overestimates the response around 995s.

5. Conclusion

The second order term of the FNV equation (equation 3) corresponding to the contribution of the linear potential integrated from the mean water level to the 1st order wave elevation was represented as a pulse load of sinusoidal shape. This simple approximation can explain the phasing and the amplitude of the responses found in the experiment. The observed oscillations appear to be the transient response to a short pulse load (of a time duration close to the eigenperiod of the structure) due to higher order hydrodynamic contributions rather than the response to a slamming load. The steady state response to the second order load term is still relevant but cannot explain extreme load responses in a close to breaking or combined breaking loading situation.

It is important to account for the right damping when assessing these maximum loads, because it defines the state (position and velocity) of the structure when it is hit by the pulse load. A strongly damped structure will most likely decay into a resting position quickly after a transient response. This will induce lower loads when a new pulse load excites it. This will be investigated in further tests with varying damping.

A commonly used method to estimate the response of a bottom-fixed offshore wind turbine to a breaking wave is to add a pulse load to the classical Morison equation (see[7]). It is shown in the present paper that none of these two models suffices to explain the first mode motion occurring after a breaking or near breaking wave hits the cylinder. The study presented brings some new insight into the process of maximum loading by showing that in order to correctly capture the first mode motion of the system, higher order excitation hydrodynamic loads are required.

No slamming model was required to match the experiments, which suggests that a slamming load occurs too rapidly to trigger the first mode motion. However, this study does not aim at replacing state of the art theoretical models for estimating maximum loads on offshore wind turbines. A more thorough analysis, especially in a statistical perspective, is required to further validate it. Furthermore, it is important to recall that the presented experiments were carried out with a single degree of freedom system, with a conservative linear mode shape and where the second mode was not modelled. The second mode motion of the structure can be excited by slamming events and may increase the maximum loads. The latter will be presented in future studies.

Acknowledgements

This study has been financed by Statkraft and the Norwegian Research Council. The authors are grateful to the support brought by Marintek during the realization of the experiments, both in terms of working hours and relevant input to the presented discussion. The model setup was originally financed by Statoil and Statkraft through the Dudgeon offshore wind project.

References

[1] M. Damgaard, L.B. Ibsen, L.V. Andersen, J.K.F. Andersen, Cross-wind modal properties of offshore wind turbines identified by full scale testing, J. Wind Eng. Ind. Aerodyn. 116 (2013) 94–108. doi:10.1016/j.jweia.2013.03.003.

[2] M. Damgaard, J.K.F. Andersen, Natural Frequency And Damping Estimation of an Offshore Wind Turbine Structure, in: International Society of Offshore and Polar Engineers, 2012. https://www.onepetro.org/conference-paper/ISOPE-I-12-126 (accessed July 9, 2015).

[3] C. Devriendt, M. El-Kafafy, G. De Sitter, P. Guillaume, Estimating damping of an offshore wind turbine using an overspeed stop and ambient excitation, in: Proc. 15th Int. Conf. Exp. Mech., 2012. http://www.vliz.be/imisdocs/publications/265470.pdf (accessed September 25, 2015).

[4] R. Shirzadeh, W. Weijtjens, P. Guillaume, C. Devriendt, The dynamics of an offshore wind turbine in parked conditions: a comparison between simulations and measurements, Wind Energy. 18 (2015) 1685–1702. doi:10.1002/we.1781.
[5] Forewind - Dogger Bank Creyke Beck, (n.d.). http://www.forewind.co.uk/projects/dogger-bank-creyke-beck.html (accessed January 19, 2016).
[6] J. Frimann-Dahl, Experimental Validation and Design Review of Wave Loads on Large-Diameter Monopiles, NTNU, Marine Technology, 2015.
[7] Environmental Conditions and Environmental Loads DNV-RP-C205, DNV, 2014.
[8] T.B. Johannessen, Nonlinear Superposition Methods Applied to Continuous Ocean Wave Spectra, J. Offshore Mech. Arct. Eng. 134 (2011) 011302–011302. doi:10.1115/1.4003518.
[9] T.B. Johannessen, On the Use of Linear and Weakly Nonlinear Wave Theory in Continuous Ocean Wave Spectra: Convergence With Respect to Frequency, (2008) 211–217. doi:10.1115/OMAE2008-57355.
[10] A.K. Jha, S.R. Winterstein, Wavemaker 2.0: Simulation and Identification of Second-Order Random Waves, 1996.
[11] O.M. Faltinsen, J.N. Newman, T. Vinje, Nonlinear wave loads on a slender vertical cylinder, J. Fluid Mech. 289 (1995) 179–198. doi:10.1017/S0022112095001297.
[12] B.J. Natvig, A Proposed Ringing Analysis Model For Higher Order Tether Response, Fourth Int. Offshore Polar Eng. Conf. (1994). https://www.onepetro.org/conference-paper/ISOPE-I-94-005 (accessed June 10, 2014).
[13] J.N. Newman, Nonlinear Scattering of Long Waves by a Vertical Cylinder, in: J. Grue, B. Gjevik, J.E. Weber (Eds.), Waves Nonlinear Process. Hydrodyn., Springer Netherlands, 1996: pp. 91–102. http://link.springer.com/chapter/10.1007/978-94-009-0253-4_8 (accessed June 23, 2014).
[14] J.R. Krokstad, C.T. Stansberg, A. Nestegård, T. Marthinsen, A New Nonslender Ringing Load Approach Verified Against Experiments, J. Offshore Mech. Arct. Eng. 120 (1998) 20–29. doi:10.1115/1.2829515.
[15] O. Faltinsen, A. Timokha, Sloshing, Cambridge University Press, 2009.
[16] O.M. Faltinsen, Sea loads on ships and offshore structures, Cambridge, 1990.
[17] J. Wienke, H. Oumeraci, Breaking wave impact force on a vertical and inclined slender pile—theoretical and large-scale model investigations, Coast. Eng. 52 (2005) 435–462. doi:10.1016/j.coastaleng.2004.12.008.
[18] J.M. Biggs, Introduction to structural dynamics, 1964.